

1 *Supporting Information for*

2 **From salinity to nanoplastics: redefining safe yield in strip-island**
3 **aquifers under emerging contaminant threats**

4 **Tianyuan Zheng^{1,2,3*}, Chunxiang Ma^{1,2,3}, Shaobo Gao^{1,2,3**}, Jian Luo⁴**

5 ¹ College of Environmental Science and Engineering, Ocean University of China,
6 Qingdao, China, Qingdao 266100, China.

7 ² Key Laboratory of Marine Environment and Ecology, Ministry of Education, Ocean
8 University of China, Qingdao 266100, China.

9 ³ Shandong Provincial Key Laboratory of Marine Engineering Geology and the
10 Environment, Ocean University of China, Qingdao 266100, China.

11 ⁴ School of Civil and Environmental Engineering, Georgia Institute of Technology,
12 Atlanta, GA 30332, USA.

13 Corresponding author: Tianyuan Zheng (zhengtianyuan@ouc.edu.cn);

14 Shaobo Gao (gaoshaobo@ouc.edu.cn)

15

16 **Contents of this file**
17 Figures S1-S5
18 Text S1-S4

19 **Introduction**

20 This supplementary material supports the main manuscript by providing detailed methodological
21 documentation, experimental validation, and additional analytical results related to the investigation of nanoplastic
22 transport in idealized strip-island aquifers. It includes comprehensive descriptions of the laboratory-scale column
23 experiments, the synthesis procedures for hydrophilic and hydrophobic nanoplastics, the calibration of numerical
24 model parameters, and the validation of simulated results against experimental data.

25 Specifically, Text S1 shows the governing equations for groundwater flow and the transport of saline solutes
26 in aquifers. Text S2 outlines the synthesis protocol for polystyrene-palladium (PS-Pd) nanoplastics with controlled
27 surface properties. Text S3 describes the column experimental setup and procedure used to characterize nanoplastic
28 transport parameters in porous media. Text S4 presents comparative simulations highlighting the differential
29 migration behavior of hydrophilic and hydrophobic nanoplastics under pumping conditions. Figures S1-S5 provide
30 schematic diagrams of experimental apparatus, conceptual models, calibration results, and comparative
31 concentration distributions that supplement the findings discussed in the main text.

32 The materials and methods presented herein are intended to ensure reproducibility, enhance transparency,
33 and facilitate the interpretation of the integrated numerical-experimental approach adopted in this study. By
34 documenting the experimental and modeling steps in detail, this supplement aims to reinforce the robustness of the
35 conclusions drawn in the main manuscript and provide a foundation for further research on nanoplastic
36 contamination in coastal groundwater systems.

37

38 **Text S1 Groundwater flow equations for the unsaturated zone and salinity transport equations**

39 The governing equation for variable-density groundwater flow in the unsaturated-saturated zone is given by
40 the Richards equation:

$$\theta \rho \frac{\partial S_w}{\partial t} + \theta S_w \frac{\partial \rho}{\partial C} \frac{\partial C}{\partial t} = \nabla \cdot \rho \left(\frac{k_r \mathbf{k}}{\mu} (\nabla P + \rho \mathbf{g} \nabla Z) \right) + \rho q_{ss} \quad (1)$$

41 where θ is the porosity [-], ρ is the fluid density [ML⁻³], S_w is the saturation [-], C is the salt
42 concentration of the fluid [ML⁻³], \mathbf{k} is the saturated permeability coefficient [LT⁻¹], k_r is the relative
43 permeability coefficient [-], μ is the dynamic viscosity [ML⁻¹T⁻¹], P is fluid pressure, varying with time
44 [ML⁻¹T⁻²], \mathbf{g} is the gravitational acceleration [LT⁻²]; Z is elevation[L], q_{ss} is the source-sink term [T⁻¹].

45 The solute transport equation, describing advective and dispersive salt migration in groundwater, conserves
46 solute mass as follows:

$$\frac{\partial S_w \theta C}{\partial t} = \nabla \cdot \rho \left[S_w D \nabla \left(\frac{C}{\rho} \right) \right] + \nabla \cdot C \frac{k_r \mathbf{k}}{\mu} \nabla P + q_{ss} C_{ss} \quad (2)$$

47 where D is the hydrodynamic dispersion coefficient [L²T⁻¹], and C_{ss} is the salt concentration of the
48 source-sink term [ML⁻³].

49 The relationship between relative permeability, capillary pressure, and phase saturation in unsaturated
50 aquifers is described by the van Genuchten curve (van Genuchten et al., 1980):

$$S_w = S_{res} + (1 - S_{res}) \left(\frac{1}{1 + (a|\psi|^n)} \right)^{\frac{n-1}{n}} \quad (3)$$

$$k_r = S_e^l \left\{ 1 - \left[1 - S_e^{n/(n-1)} \right]^{(n-1)/n} \right\}^2 \quad (4)$$

$$S_e = \frac{S_w - S_{res}}{1 - S_{res}} \quad (5)$$

51 where S_{res} is the residual water saturation [-], a , n and l is the corresponding constants [-], S_e is the
52 effective water saturation [-].

53

54 **Text S2 Synthesis of Hydrophilic and Hydrophobic nanoplastics**

55 Poly(styrene) nanoparticles loaded with palladium (PS-Pd NPs) were synthesised via a two-step emulsion
56 polymerisation method, comprising core formation and shell construction stages. First, 12.0 g of acrylonitrile (AN),
57 0.36 g of sodium dodecyl sulphate (SDS), and 0.36 g of potassium perpolysulphate (KPS) were added to a reaction
58 vessel containing 108.0 g of deionised water (60°C). The mixture was stirred at 300 rpm until complete dissolution.
59 Continuous nitrogen gas was introduced to eliminate oxygen from the reaction system. Subsequently, 0.24 g of
60 potassium polyethylene glycol 4-nonylphenyl 3-sulfonylpropyl ether (KPE) and 0.18 g of K_2PdCl_4 , each dissolved
61 in 8.0 mL of deionised water, were added to the reaction vessel via syringe over 2 minutes. The mixture reacted at
62 60°C for 40 minutes to form the polymer core.

63 Whilst the core reaction proceeds continuously, the monomer composition within the reaction system is
64 gradually modulated via two peristaltic pumps and two feeders (Feeder 1 and Feeder 2), thereby achieving the
65 transition from the AN core to the styrene shell. Feeder 1 was supplemented with styrene, AN, and deionised water;
66 Feeder 2 contained styrene, SDS, divinylbenzene (DVB), and deionised water. The specific quantities of reagents
67 used in the synthesis of PS-Pd-1 and PS-Pd-2 are listed in Table S1. Additionally, an appropriate amount of KPS
68 (PS-Pd-1: 0.18 g; PS-Pd-2: 0.09 g) was dissolved in 4.0 g of deionised water and directly injected into the reaction
69 vessel.

70 Activate the peristaltic pump (flow rate 0.02 mL/min) to transfer the solution from Feeder 2 into Feeder 1,
71 and subsequently from Feeder 1 into the reaction vessel. This process shall continue for 2 hours. Thereafter,
72 remove Feeder 1 and directly inject the solution from Feeder 2 into the reaction system, allowing the reaction to
73 proceed for a further 0.5 hours. Following removal of Feeder 2, the reaction mixture shall continue to react within
74 the vessel for an additional 2 hours. Finally, add 20.0 g of deionised water and react for 10 minutes to terminate the
75 polymerisation.

76 Upon completion of the reaction, remove the vessel from the oil bath. Centrifuge the resulting product five
77 times with ethanol (5000 rpm, 10 minutes per run). Place the centrifuged precipitate in deionised water for dialysis
78 over three days, replacing the dialysis buffer daily. All reagents used in the experiment were purchased from Sigma
79 Aldrich.

80 **Text S3 Column Experiment**

81 Column experiments were conducted according to previously reported methodologies for studying
82 nanoplastics migration in sediments, with the experimental apparatus schematic shown in Figure 1. The packed
83 column was first pre-equilibrated using deionised water, followed by the injection of 20 column volumes (PV) of
84 artificial seawater as background solution at a flow rate of 4.0 mL/min. Subsequently, 5 PV of a 10 mg/L
85 nanoplastic suspension was injected at the same flow rate, followed by elution with an additional 5 PV of seawater.
86 To prevent sedimentation of nanoplastic particles, the suspension was continuously homogenised during injection
87 via a magnetic stirrer.

88 During the migration experiment, effluent samples were collected every 10 minutes. The concentration of
89 palladium (Pd) in these samples was determined using inductively coupled plasma mass spectrometry (ICP-MS).
90 Based on this, quantitative calibration curves for the concentrations of PS-Pd-1 and PS-Pd-2 nanoplastics in
91 seawater were established, enabling quantitative analysis of the migration behaviour of the nanoplastics. By
92 adjusting the parameters, the simulation results achieved high consistency with the experimental results in the
93 breakthrough curve. ($R^2 > 9.0$)

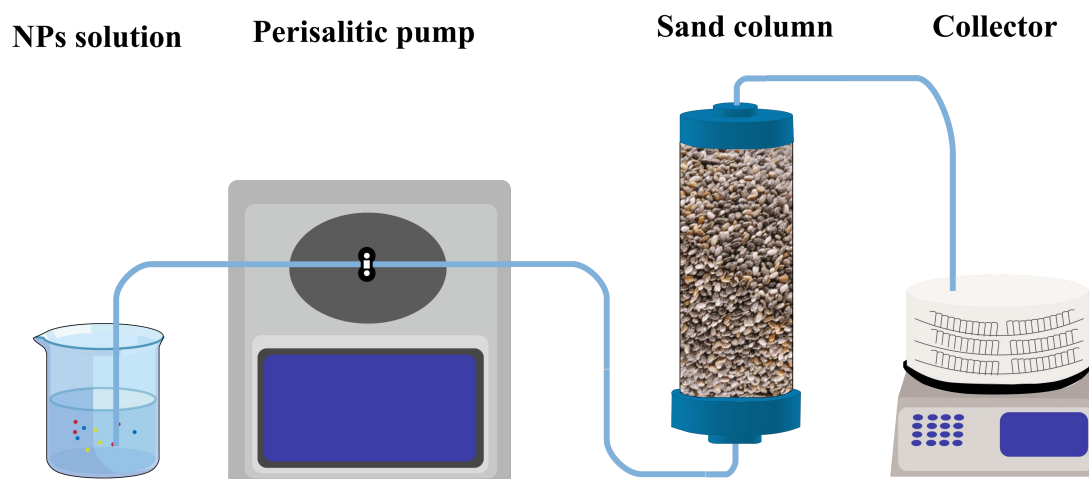
94 **Text S4 Column Experiment**

95 Laboratory-scale deep extraction simulations revealed distinct spatiotemporal distribution differences
96 between hydrophilic (PS-Pd-1) and hydrophobic (PS-Pd-2) nanoplastics (NPs) during the initial stress period, with
97 such variations governed by the intrinsic surface properties of NPs that modulate their adsorption interactions with
98 aquifer solid media. The initial spatial distributions of the two MP types (Fig. S5(a₁, b₁)) characterize the
99 occurrence pattern of NPs in groundwater subsequent to freshwater lens formation, while their temporal evolution
100 profiles (Fig. S5(a₂-a₄), (b₂-b₄)) demonstrate a rapid expansion of the PS-Pd-2 plume, verifying its superior
101 mobility—this is attributed to weak electrostatic and van der Waals forces between hydrophobic PS-Pd-2 and
102 aquifer solids, which minimize particulate retention and facilitate advective transport. Notably, the contamination
103 area of PS-Pd-2 reached 29.6% under initial conditions, exactly twice that of PS-Pd-1 (14.8%). Under pumping
104 conditions, their distribution patterns showed significant divergence: PS-Pd-1 and PS-Pd-2 covered 17.1% and
105 43.5% of the reconfigured freshwater lens area, respectively. Hydrophobic PS-Pd-2 presented broader liquid-phase
106 retention in the freshwater lens due to its stronger dispersion properties, whereas hydrophilic PS-Pd-1 exhibited
107 enhanced solid-phase adsorption driven by its high surface energy, resulting in pronounced solid-phase
108 accumulation and a reduced fraction in the mobile aqueous phase. MP concentrations decreased by approximately
109 50% on average in the central lens region below the mid-lens area, with no such attenuation in the high-flow
110 seawater exchange zones on both sides, where intensified advective transport counteracts the reduction of MP
111 concentrations.

112 Hydrophobic PS-Pd-2 consistently exhibited a more extensive spatial distribution and a stronger
113 accumulation tendency in the groundwater system during pumping (Fig. S5), a phenomenon synergistically
114 induced by its inherent physicochemical properties and pumping-triggered hydrodynamic perturbations. Its low
115 surface hydrophilicity weakens solid-phase retention, sustaining high mobility in the aqueous phase, while the
116 radial flow generated by pumping further drives the migration and enrichment of PS-Pd-2 toward the pumping
117 well. During pumping operations, the 1% C_{nps} isoconcentration line of hydrophobic NPs exceeded the wellhead
118 within 3 minutes, whereas that of hydrophilic NPs never reached the well height at any time, as PS-Pd-1 was
119 immobilized by irreversible solid-phase adsorption onto aquifer media. Notably, the freshwater lens contracted
120 rapidly and reached stability within 3 minutes in simulations with hydrophilic NPs; this accelerated contraction
121 originated from the solid-phase adsorption of PS-Pd-1, which caused pore blockage in the aquifer, altered its
122 hydraulic conductivity, and thus inhibited groundwater recharge to the lens. The environmental hazards of

123 hydrophobic NPs stem not only from their physical impacts as particulate matter but also from their role as
124 efficient toxicant carriers—their low surface free energy enables the adsorption, concentration and subsequent
125 release of various toxic chemicals in biological organisms, inducing combined toxic effects.

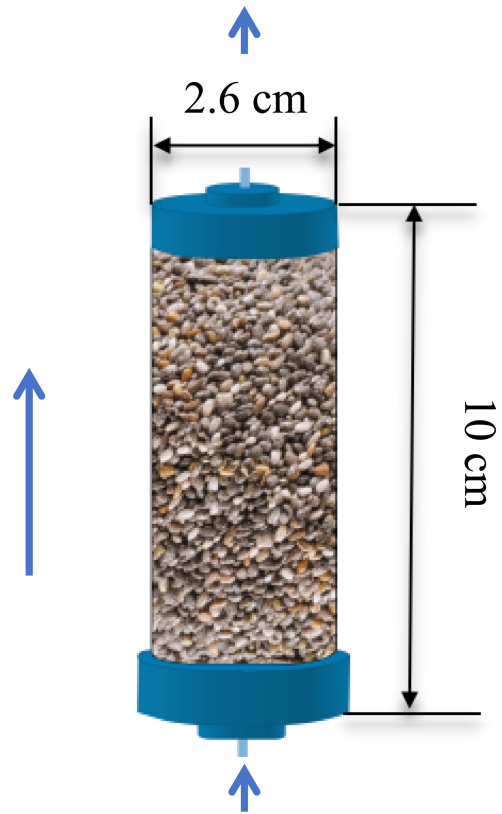
126



127

128

Fig. S1. Column Experiment Apparatus



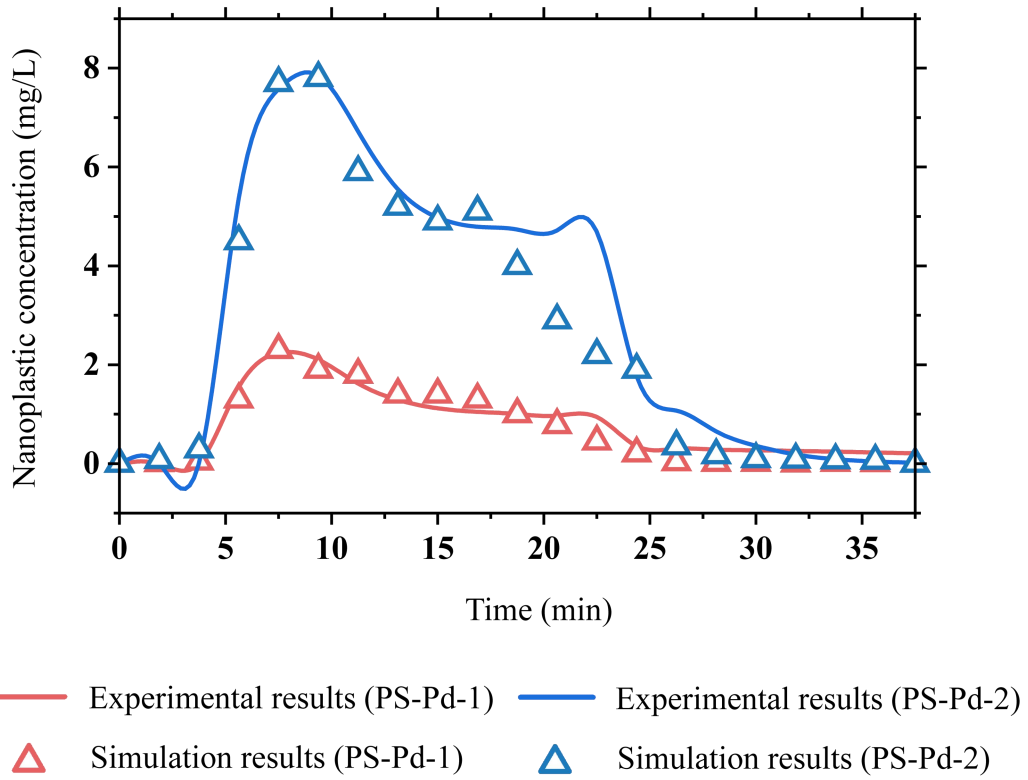
$$C_{\text{nps}} = [10 \text{ mg/L}]/\text{Nm}$$

$$C_s = 35 \text{ mg/L}$$

129

130

Fig. S2. Column Experiment Conceptual Model



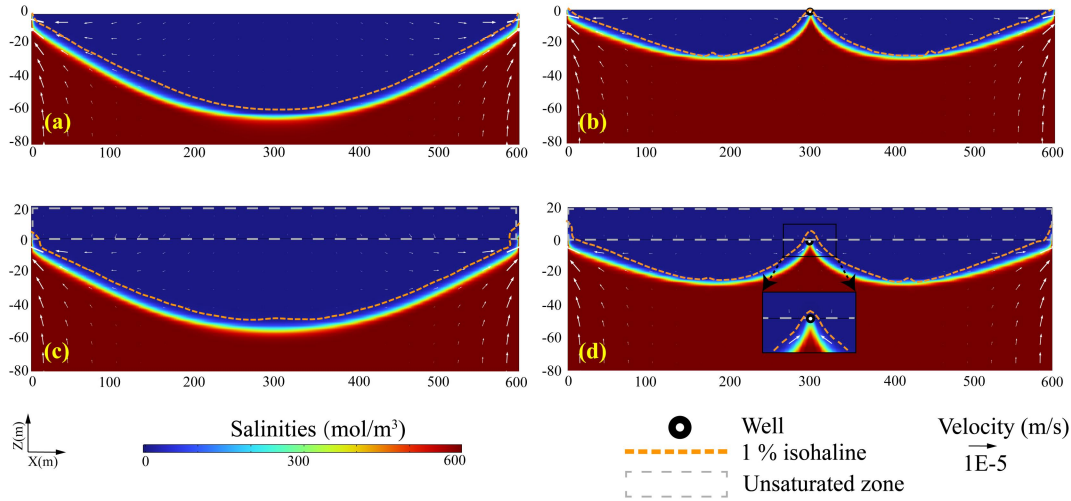
131

132

Fig. S3. Concentrations obtained through column experiments versus numerical simulation results approximated

133

by adjusting nanoplastic migration parameters



134

135 **Fig. S4.** Simulation results for freshwater lens formation and central-apex pumping in island aquifers: (a) and (b)

136 respectively depict the freshwater lens formation stage and central-apex pumping conditions simulated within Tang

137 et al.'s numerical reference scenario, with results extracted from the upper 80 m aquifer; (c) and (d) present

138 scaled-up simulations of the freshwater lens formation stage and the freshwater lens under mid-top pumping

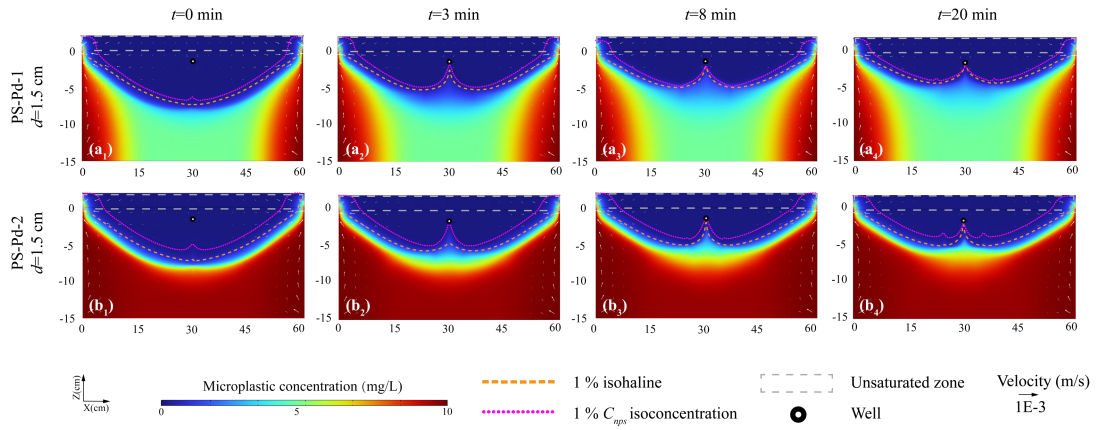
139 conditions, respectively, incorporating an unsaturated zone added to Tang et al.'s reference control experiment

140 setup. Results cover the 80 m saturated aquifer and the overlying 20 m unsaturated zone. The yellow dashed line

141 denotes the 1% isohaline. The black-framed section, indicated by black arrowed dashed lines, represents an

142 enlarged view of the wellhead vicinity. The black-edged white dot marks the extraction wellhead location at the

143 uppermost 0 m of the saturated zone, precisely at the island's centre.



145

146 **Fig. S5.** Simulated nanoplastic concentrations in laboratory-scale idealized strip island aquifers during pumping:147 (a₁/a₂/a₃/a₄) Concentration distributions of hydrophilic nanoplastics (PS-Pd-1) and (b₁/b₂/b₃/b₄) hydrophobic148 nanoplastics (PS-Pd-2) at 0, 3, 8, and 20 minutes post-pumping. Orange dashed lines represent the 1% C_{nps}

149 isoconcentration lines, pink dotted lines represent the 1% isohalines, and gray shaded areas represent the

150 unsaturated zone.

151